Family of binary transition metal pnictide superconductors

Zheng-Wei Liao,[1] Xin-Wei Yi,[1] Jing-Yang You,[2,*] Bo Gu,[3,†] and Gang Su[1,3,‡]

[1]*School of Physical Sciences, University of Chinese Academy of Sciences, Beijing 100049, China*

[2]*Department of Physics, National University of Singapore, 2 Science Drive 3, Singapore 117551*

[3]*Kavli Institute for Theoretical Sciences, CAS Center for Excellence in Topological Quantum Computation, University of Chinese Academy of Sciences, Beijing 100190, China*

(Received 21 August 2022; revised 28 March 2023; accepted 5 June 2023; published 6 July 2023)

Superconductivity in transition metal nitrides (TMNs) has been investigated for a long time, such as zirconium nitride (ZrN) with a superconducting transition temperature T_c of 10 K. Recently, a phase diagram has been revealed in ZrN_x with different nitrogen concentrations, which is very similar to that of high-temperature copper oxide superconductors. Here, we study the TMNs with a face-centered cubic lattice where ZrN and HfN have been experimentally obtained and predict eight new stable superconductors by the first-principles calculations. We find that CuN has a high T_c of 30 K with a very strong electron-phonon coupling (EPC) strength. In contrast to ZrN, CuN has softening acoustic phonons at the high-symmetry point L, which accounts for its much stronger EPC. In addition, the highly symmetrical structure leads to topological nodal points and lines, such as the hourglass Weyl loop on the $k_{x/y/z} = 0$ plane and Weyl points on the $k_{x/y/z} = 2\pi/a$ plane, as well as quadratic band touch at the Γ point. CuN could be a topological superconductor. Our results expand the transition metal nitrides superconductor family and would be helpful to guide the search for high-temperature topological superconductors.

DOI: 10.1103/PhysRevB.108.014501

I. INTRODUCTION

Transition metal nitrides (TMNs) as a class of materials with excellent physical properties, such as high hardness and strength, strong corrosion resistance, high melting point, good chemical and thermal stability [1–5], have attracted extensive attention and wide applications in various fields [6–10]. In addition, many TMNs exhibit superconductivity [11,12]. Since the 1930s, many TMN superconductors have been discovered. Nitrogen atoms in these superconductors provide strong bonding and large electron-phonon coupling (EPC), resulting in superconductivity [13]. For instance, ZrN is a typical TMN superconductor, which displays the highest superconducting transition temperature T_c of 10.0 K among the IV^B TMNs [14,15]. As a hard metal nitride superconductor, ZrN is suitable for applications under extreme working conditions, whereas most materials with superior mechanical strength and hardness are semiconductors or insulators, which lack metallicity and superconductivity [16]. A recent theoretical study has shown that under tensile strain along the high-symmetry crystallographic [001] direction, T_c of ZrN can reach 17.1 K [17]. Several other TMN superconductors have been reported including TiN with a maximal T_c of 6.0 K [18], HfN with a T_c of 8.8 K [19], VN with a T_c of 8 to 9 K [20], NbN with a T_c of 17 to 18 K [20], TaN with a T_c of 10.8 K [21], and W_2N with a T_c of 1.3 K [20]. MoN has been predicted to have the high T_c since 1981 [11,22]. A high T_c of 30 K was theoretically predicted in MoN, but the low T_c of 5–14 K were obtained in the experiments [23–26] where the obtained MoN samples were not pure and often contaminated with Mo_2N, $\gamma - Mo_2N$, Mo, or even MoO_x phases.

In addition, studies have shown that the doping has a great impact on the superconductivity in TMNs. For example, the T_c of $TiN_{0.995}$, $TiN_{0.95}$, $TiN_{0.8}$, and $TiN_{0.55}$ are 6.0, 1.7, 1.5, and 1.2 K, respectively [27]. Pure VN, 0.5% B-doped VN, 0.5% La-doped VN, 0.2% B, and La each co-doped VN, and 0.5% B and La each co-doped VN have the T_c of 9.2, 8.0, 7.8, 8.2 and 5.6 K, respectively [28–30]. ZrN_x with different nitrogen concentrations has been synthesized recently. Although ZrN_x is generally believed to obey the BCS superconducting mechanism, the phase diagram of ZrN_x is very similar to that of high-T_c copper oxide superconductors, indicating the possible relation between high-temperature superconductivity and ZrN_x [31].

In this article, we study the face-centered cubic (fcc) TMN in which ZrN and HfN have been experimentally reported. By substituting elements, eight new stable superconductors have been predicted through first-principles calculations. Interestingly, we found that CuN has a high T_c of 30 K with a very strong EPC of 3.099. In contrast to ZrN, CuN has softening acoustic phonons at the high-symmetry point L, which accounts for its much stronger EPC. In addition, the highly symmetrical structure leads to topological nodal points and lines, such as the hourglass Weyl loop on the $k_{x/y/z} = 0$ plane and Weyl points on the $k_{x/y/z} = 2\pi/a$ plane, as well as the quadratic band touch at the Γ point.

*phyjyy@nus.edu.sg
†gubo@ucas.ac.cn
‡gsu@ucas.ac.cn

II. CALCULATION METHOD

The first-principles calculations were based on the density-functional theory (DFT) as implemented in the Vienna *ab initio* (VASP) [32] and QUANTUM-ESPRESSO (QE) packages [33], with the projector augmented-wave method [34]. VASP was used to optimize the structure until the forces on atoms were less than 1 meV/Å, and to calculate the electronic band structure, within the Perdew-Burke-Ernzerhof parametrization of the generalized gradient approximation [35]. The plane-wave cutoff energy was taken as 500 eV. The Monkhorst-Pack scheme was used to sample the Brillouin zone (BZ) with a **k** mesh of $15 \times 15 \times 15$. The calculations of phonon spectra and superconducting properties were performed using QE within density-functional perturbation theory [36] and the Vanderbilt-type ultrasoft potentials [37]. The plane-wave kinetic-energy cutoff was set as 100 Ry and the **q**-point mesh in the first BZ was taken as $4 \times 4 \times 4$. An unshifted **k**-point mesh of $36 \times 36 \times 36$ was utilized. The convergence of calculations is discussed in the Supplemental Material [38]. For EPC calculations, the Methfessel-Paxton smearing method [39] with a smearing value of 0.015 Ry was taken.

The BCS theory states that the strength of EPC of a material directly affects its superconducting transition temperature. According to Migdal-Eliashberg theory [40,41], the EPC parameter λ_{qv} can be calculated by

$$\lambda_{qv} = \frac{\gamma_{qv}}{\pi h N(E_F)\omega_{qv}^2}, \tag{1}$$

where γ_{qv} is the phonon linewidth, ω_{qv} is the phonon frequency, and $N(E_F)$ is the electronic density of states at the Fermi level. γ_{qv} can be estimated by

$$\gamma_{qv} = \frac{2\pi\omega_{qv}}{\Omega_{BZ}} \sum_{k,n,m} \left|g^v_{kn,k+qm}\right|^2 \delta(\epsilon_{kn} - \epsilon_F)\delta(\epsilon_{k+qm} - \epsilon_F), \tag{2}$$

where Ω_{BZ} is the volume of the BZ, ϵ_{kn} and ϵ_{k+qm} denote the Kohn-Sham energy, and $g^v_{kn,k+qm}$ represents the EPC matrix element, which describes the probability amplitude for the scattering of an electron with a transfer of crystal momentum q and can be obtained self-consistently by the linear-response theory [42]. The Eliashberg electron-phonon spectral function $\alpha^2F(\omega)$, and the cumulative frequency-dependent EPC $\lambda(\omega)$ can be calculated by

$$\alpha^2F(\omega) = \frac{1}{2\pi N(E_F)} \sum_{qv} \frac{\gamma_{qv}}{\omega_{qv}} \delta(\omega - \omega_{qv}), \tag{3}$$

and

$$\lambda(\omega) = 2\int_0^{\omega} \frac{\alpha^2F(\omega)}{\omega} d\omega, \tag{4}$$

respectively.

Utilizing the calculated $\alpha^2F(\omega)$ and $\lambda(\omega)$ together with a typical value of the effective screened Coulomb repulsion constant $\mu^* = 0.1$, we calculate the logarithmic average frequency $\omega_{\log}$ by

$$\omega_{\log} = \exp\left[\frac{2}{\lambda}\int_0^{\infty} \frac{d\omega}{\omega}\alpha^2F(\omega)\log\,\omega\right]. \tag{5}$$

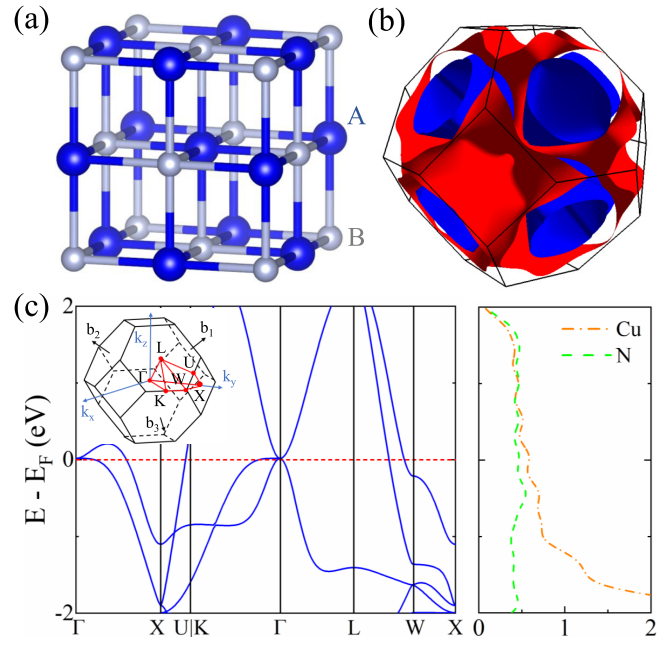

FIG. 1. (a) The conventional cell of face-centered cubic lattice AB. (b) The Fermi surface, (c) electronic band structure and projected density of states of CuN.

The superconducting transition temperature T_c can be obtained by

$$T_c = \frac{\omega_{\log}}{1.2}\exp\left[-\frac{1.04(1+\lambda)}{\lambda - \mu^*(1+0.62\lambda)}\right]. \tag{6}$$

When λ is larger than 1.5, two separate correction factors for "strong-coupling correction" f_1 and "shape correction" f_2 should be considered, which involve one additional parameter [42],

$$\overline{\omega}_2 = \langle\omega^2\rangle^{1/2} = \left[\frac{2}{\lambda}\int_0^{\infty} \alpha^2F(\omega)\omega\, d\omega\right]^{1/2}. \tag{7}$$

And the T_c for $\lambda > 1.5$ can be obtained by

$$T_c = \frac{f_1 f_2 \omega_{\log}}{1.2}\exp\left[-\frac{1.04(1+\lambda)}{\lambda - \mu^*(1+0.62\lambda)}\right], \tag{8}$$

where

$$f_1 = \left[1 + \left[\frac{\lambda}{2.46(1+3.8\mu^*)}\right]^{3/2}\right]^{1/3},$$
$$f_2 = 1 + \frac{(\overline{\omega}_2/\omega_{\log} - 1)\lambda^2}{\lambda^2 + [1.82(1+6.3\mu^*)(\overline{\omega}_2/\omega_{\log})]^2}. \tag{9}$$

III. RESULTS OF CuN

As shown in Fig. 1(a), ZrN has a NaCl-type fcc lattice with the $Fm\bar{3}m$ space group. By substituting Zr with other transition metal elements and N with other VA group elements, we have obtained eight new structurally stable transition metal pnictide superconductors by the DFT calculations, including CdN, CdP, CdAs, CuN, CuSb, HfP, HgSb, and ZnSb. Using the McMillan-Allen-Dynes approach [42,43] based on the BCS theory with a typical Coulomb repulsion value of

TABLE I. The calculated total EPC λ, $\omega_{\log}$, T_c of our proposed new stable compounds as well as two experimentally synthesized materials HfN and ZrN for comparison.

	λ	$\omega_{\log}$ (K)	T_c (K)	$T_c^{\text{exp.}}$ (K)
CdN	1.314	199.5	19.86	
CdP	1.266	122.0	11.64	
CdAs	1.426	94.9	10.29	
CuN	3.099	124.2	29.64	
CuSb	1.016	84.5	6.03	
HfN	0.658	305.9	9.10	8.8 [19]
HfP	0.670	151.8	4.74	
HgSb	0.956	85.9	5.57	
ZnSb	1.387	93.0	9.81	
ZrN	0.657	375.3	10.65	10.0 [14,15]

$\mu^* = 0.1$, we calculate the T_c, EPC stength λ, and logarithmic average frequency $\omega_{\log}$ of these superconductors as listed in Table I. As shown in Sec. S2 of the Supplemental Material [38], the total EPC λ, and T_c for the proposed compounds in our paper are slightly modified by the spin-orbit coupling (SOC). In addition, we also calculate the T_c of two experimentally reported TMN superconductors ZrN and HfN, which are 10.93 and 9.1 K, respectively, close to the experimental T_c of 10 and 8.8 K. Among these stable fcc TMN superconductors, CuN has the strongest EPC, and the highest T_c of 30 K among other TMNs. For CuN, we tried to use CALYPSO [44] to search possible stable structures and found that the structures with the lowest enthalpy predicted by CALYPSO are $P1$ space group, not the $Fm\bar{3}m$ discussed in our paper. Our calculations show that these $P1$ structures have imaginary frequency modes in the phonon spectra, indicating the dynamic instability. It is noted that Cu_3N [45] with space-group $Pm\bar{3}m$ and CuN_8 [46] with space-group $Pnma$ have been obtained in experiments. The formation energies of Cu_3N and CuN_8 is 0.80 and 1.24 eV/atom above the hull, respectively [47]. These values are near and even higher than that of CuN (0.84 eV/atom) [47]. Thus, it is also possible to obtain $Fm\bar{3}m$ CuN in a future experiment. In the following, we studied CuN as an example in detail.

A. Crystal structure of CuN

The optimized lattice constant of CuN is 4.177 Å. Figure 1(b) gives the Fermi surface of CuN where red and blue surfaces represent the different bands crossing the Fermi surface, which obviously accords with the crystal symmetry of this structure. Figure 1(c) shows the band structure along the high-symmetry paths $\Gamma - X - U|K\text{-}\Gamma - L - W - X$ and projected density of states (DOS) of CuN, which show the metallic property with nearly equal contribution of Cu and N atoms near the Fermi level.

B. Electronic and topological properties of CuN

Because of the highly symmetric crystal structure, this material can exhibit many interesting topological properties in the band structure [48,49]. Figure 2(a) shows the shape of the nodal loop obtained from the DFT calculations on the $k_z = 0$ plane within the BZ. Similarly, other two nodal

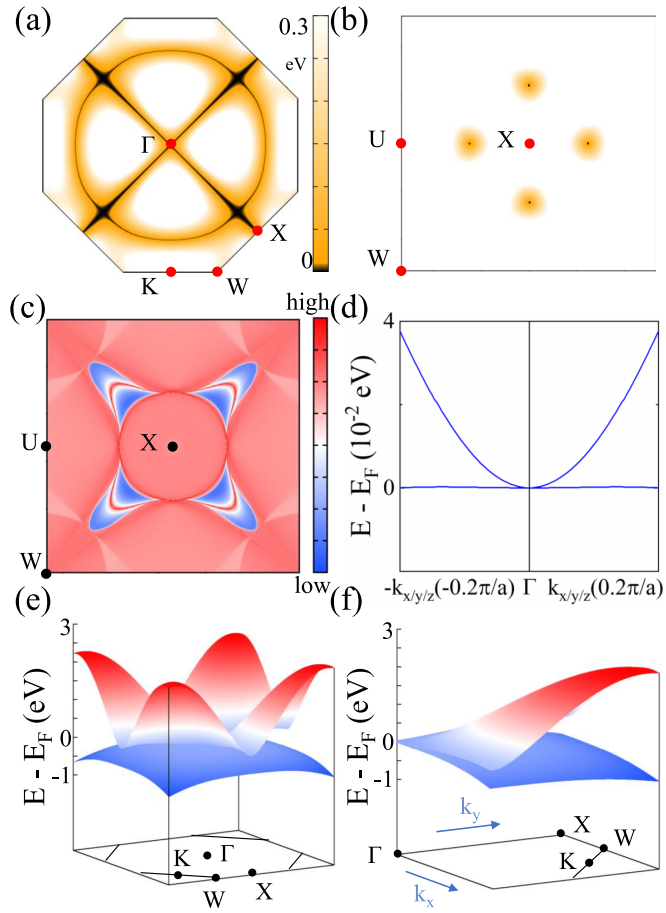

FIG. 2. (a) Shape of the Weyl loop on the $k_z = 0$ plane and (b) the distribution of Weyl points on the $k_y = 2\pi/a$ plane for CuN. (c) The isoenergy slice at 0.8 eV projected along the k_y direction of CuN. (d) The quadratic band dispersion around Γ point. (e) $E(k_x, k_y)$ on the $k_z = 0$ plane, and (f) $E(k_x, k_y)$ on a quarter of the $k_z = 0$ plane of CuN.

loops appearing on $k_x = 0$ and $k_y = 0$ planes can also be obtained by symmetry. In Fig. 2(c), we plot the constant energy slice at −0.8 eV, which cuts through the drumhead states, forming a few arcs. In Fig. 1(c), we can find the band crossing point along the $U - X$ path. The bands possess different irreducible representations of C_2 rotation symmetry and time-reversal symmetry by first-principles calculations. It is a nontrivial band crossing, leading to a nodal Weyl point. Since the fourfold rotation symmetry along $\Gamma - X$, there should exist another three Weyl points on the $k_y = 2\pi/a$ plane, which has been shown in Fig. 2(b). In addition, the band dispersion around Γ points is quadratic along all three directions in k space as shown in Fig. 2(d) as well as Fig. 2(f), indicating that CuN possesses the quadratic contact point Γ protected by the crystalline symmetry [50]. As discussed in Sec. S2 of the Supplemental Material [38], the Weyl point is protected by the C_2 rotation symmetry and time-reversal symmetry and is robust against the effect of SOC.

C. Superconductivity and pressure effect of CuN

Topological superconductor with Majorana fermions is important and attractive in many fields, such as quantum

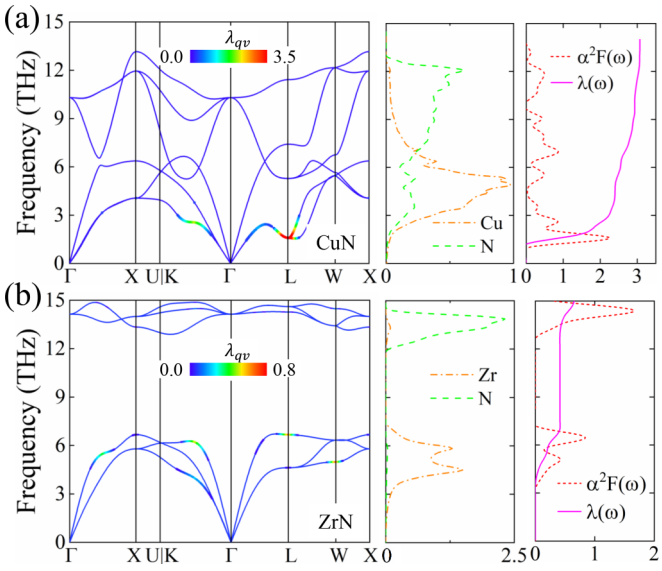

FIG. 3. The phonon spectra weighted by the magnitude of EPC λ_{qv}, projected phonon density of states, Eliashberg spectral function $\alpha^2F(\omega)$, and cumulative frequency-dependent EPC $\lambda(\omega)$ of (a) CuN and (b) ZrN.

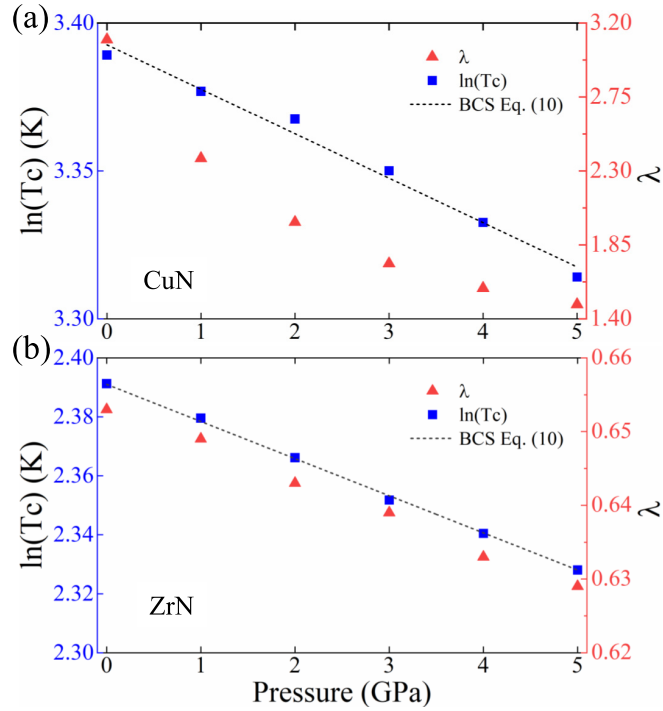

FIG. 4. Pressure-dependent logarithmic T_c and λ of (a) CuN and (b) ZrN. The dashed line is the fitting according to BCS theory.

computing [51]. The coexistence of superconductivity and nontrivial band topology in a system is crucial for the realization of topological superconductivity, which is rarely reported [52–56]. Meanwhile, the T_c of those systems is generally low. Thus, it is worthwhile to investigate the superconducing properties in the topological CuN. In Fig. 3, we study the phonon spectra weighted by the magnitude of EPC λ_{qv}, projected phonon DOS, Eliashberg spectral function $\alpha^2F(\omega)$, and cumulative frequency-dependent EPC $\lambda(\omega)$ for CuN and ZrN. For CuN, the vibration modes can be divided into two parts: low-frequency modes lower than 8 THz contributed by both Cu and N atoms and high-frequency modes higher than 8 THz dominated by vibration of N atoms. For ZrN, the vibration modes can also be divided into two parts: low-frequency modes and high-frequency modes dominated by Zr and N atoms, respectively. Between the two frequency ranges of ZrN, there is a 4.5 THz phonon gap. It is worth noting that at the high-symmetry point L, the acoustic phonons of CuN exhibit obvious softening, accounting for about 83% of the total EPC ($\lambda = 3.099$) below 6 THz, whereas ZrN has no softening acoustic phonons, and the vibration modes of Zr atom below 7.5 THz only account for 63% of the total EPC ($\lambda = 0.657$) below 7.5 THz. Softening acoustic phonons are the main source for the large EPC in CuN. At point L, the vibrations of N atoms appear to be the main reason for the softening acoustic phonons as shown in Sec. S4 of the Supplemental Material [38].

Figure 4 gives pressure dependence of logarithmic T_c and EPC λ of CuN and ZrN, respectively. Their detailed calculation results are listed in Table II. In the calculation of structural optimization, an energy term $E = V * P$ is added to the total energy, and the pressure P is added to the diagonal part of the stress tensor. In this way, the optimized structure is determined for a target pressure. It can be seen that with increasing pressure, the EPC λ of both CuN and ZrN decrease, resulting in the decrease in T_c. The calculated dT_c/dP of ZrN is −0.133 K/GPa, which is close to the experimental result of −0.17 K/GPa [57]. Based on the BCS theory, $T_c(P)$ obeys the following relationship [58]:

$$\frac{d\ln T_c}{d\ln V} = -B\frac{d\ln T_c}{dP} = -\gamma + \Delta\left\{\frac{d\ln\eta}{d\ln V} + 2\gamma\right\}, \qquad (10)$$

where B is the bulk modulus, $\gamma \equiv -d\ln\langle\omega\rangle/d\ln V$ is the Grüneisen parameter, $\eta \equiv N(E_F)\langle I^2\rangle$ is the Hopfield parameter [59] with $\langle I^2\rangle$ as the square of the electron-phonon matrix element averaged over the Fermi surface, and $\Delta \equiv 1.04\lambda(1+0.38\,\mu^*)[\lambda-\mu^*(1+0.62\,\lambda)]^{-2}$. Because

TABLE II. The DOS at Fermi level $N(E_F)$ (in unit of states/spin/eV/cell), volume of primitive cell V (Å^3), $\omega_{\log}$ (K), λ, and T_c (K) for CuN and ZrN as a function of pressure.

	P(GPa)	$N(E_F)$	V(Å^3)	$\omega_{\log}$(K)	λ	T_c (K)
CuN	0	8.19	18.22	124.2	3.099	29.64
	1	8.15	18.14	154.3	2.377	29.28
	2	8.10	18.05	180.1	1.989	29.01
	3	8.07	17.97	202.0	1.737	28.50
	4	8.03	17.89	217.7	1.587	28.01
	5	7.99	17.81	229.1	1.488	27.50
ZrN	0	4.47	24.24	375.3	0.653	10.93
	1	4.45	24.15	377.3	0.649	10.80
	2	4.43	24.05	381.5	0.643	10.66
	3	4.41	23.96	384.7	0.639	10.50
	4	4.39	23.87	387.9	0.633	10.39
	5	4.38	23.78	391.0	0.629	10.26

TABLE III. The optimized lattice constants of seven $Fm\bar{3}m$ structures CdN, CdP, CdAs, CuSb, HfP, HgSb, and ZnSb.

	CdN	CdP	CdAs	CuSb	HfP	HgSb	ZnSb
a(Å)	4.72	5.47	5.64	5.15	5.23	6.03	5.65

the first term on the right-hand side of Eq. (10) is smaller than the second term [60], the sign of dT_c/dP is mainly determined by the relative magnitude of the two terms in curly brackets in Eq. (10). The Grüneisen parameter (γ) can be directly obtained from Table II, and the Hopfield term can be determined by Eq. (10). It can be observed that our calculated results for ZrN are in perfect agreement with Eq. (10). For CuN, our calculated, $\ln T_c/dP = -0.018$ K/GPa from Eq. (10) is also comparable with the fitting slope −0.015 K/GPa in Fig. 4(a).

Topological superconductor can be achieved through the proximity effect. There are several approaches to realize the proximity effect, including the heterostructures of s-wave superconductors and topological insulators, the heterostructures of s-wave superconductors and semiconductors with strong SOC and the intrinsic materials with bulk superconductivity and surface topological Dirac cones. For the last approach, the intrinsic materials reported in experiments include the iron-based superconductors [61–68] and the recent kagome superconductor CsV_3Sb_5 [69]. In our paper, CuN has a T_c of 30 K and the topological surface states at −0.8 eV below the Fermi level. Because the Fermi level can be shifted to the position of the topological surface states by hole doping, it is promising to obtain the topological superconductor due to the proximity effect with bulk superconductivity and topological surface states.

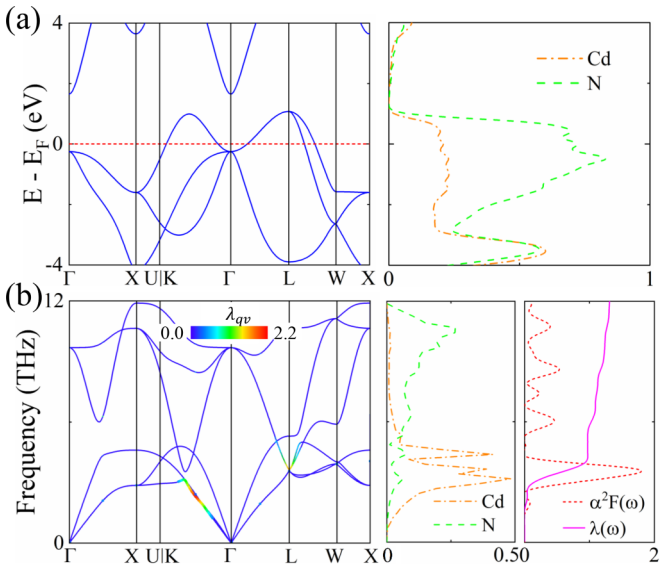

FIG. 5. (a) The electronic band structure, projected DOS, (b) the phonon spectra, projected DOS, Eliashberg spectral function $\alpha^2F(\omega)$, and the cumulative frequency-dependent EPC $\lambda(\omega)$ of CdN.

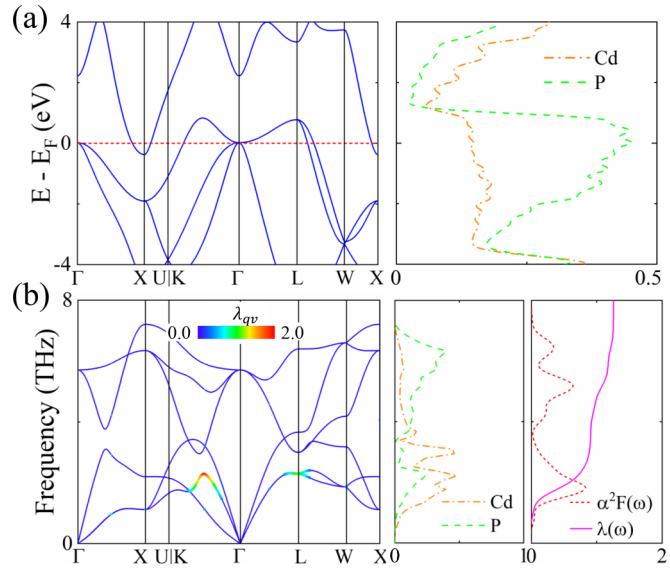

FIG. 6. Same as Fig. 5 but for CdP.

IV. SUPERCONDUCTIVITY OF OTHER STRUCTURES

In addition to CuN, the other seven superconducting materials have also been predicted. Through DFT calculations, we have obtained the optimized lattice constants for these seven materials as listed in Table III. Figure 5 depicts the electronic properties, phonon spectra, and EPC λ of CdN. Near the Fermi level, the electronic DOS of N atoms is much larger than that of Cd atoms, which is different from CuN in Fig. 3. Due to the similar vibration modes of CdN and CuN, the main sources of EPC λ in CdN are also from the point L and high-symmetry path $K - \Gamma$ in the low-frequency region. As shown in Fig. 6, CdP is similar to CdN in electronic and superconducting properties. The electronic DOS of P atoms is about three times that of Cd atoms near the Fermi surface, and the low-frequency vibration modes account for the main part of the total EPC. The results of CdAs are given in Fig. 7. Its

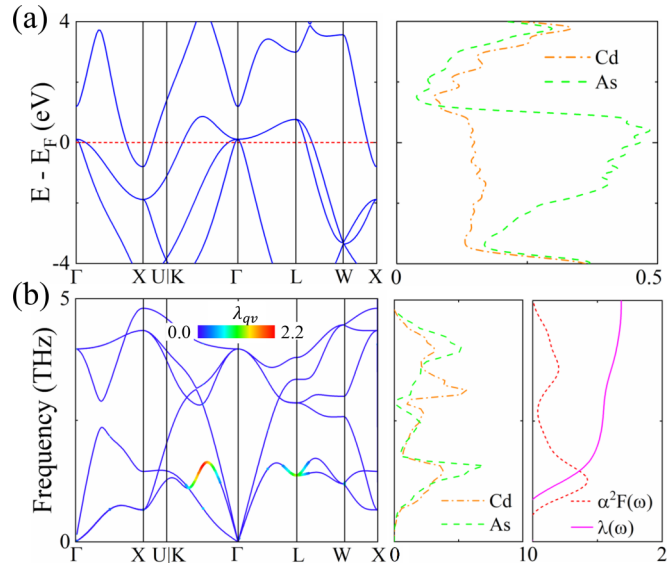

FIG. 7. Same as Fig. 5 but for CdAs.

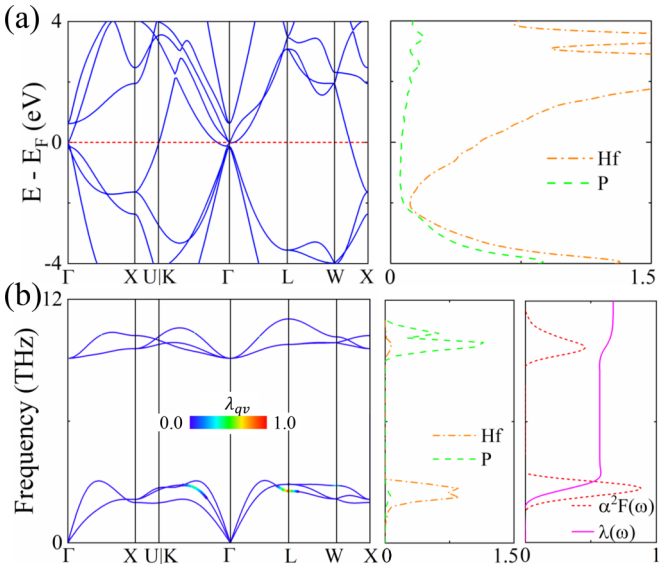

FIG. 8. Same as Fig. 5 but for HfP.

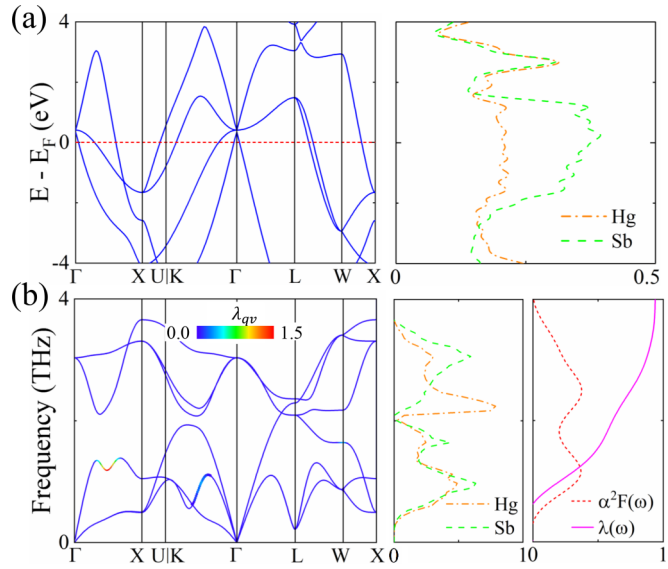

FIG. 10. Same as Fig. 5 but for HgSb.

behaviors are very similar to those of CdN and CdP, except that the phonon DOS of As atoms around 2 THz is greater than that of Cd atoms. The results of HfP are plotted in Fig. 8. Unlike CdN, CdP, and CdAs, where the electronic DOS of the anion is dominant near the Fermi level, the electronic DOS of Hf atoms is preponderant in HfP, and considerable phonon DOS at low frequency is obtained.

The results of CuSb are given in Fig. 9. The low-frequency vibration region is mainly contributed by anion Sb atoms, whereas the high-frequency region is dominated by Cu atoms. The main sources of EPC λ are from point W, high-symmetry path $K-\Gamma$, and $\Gamma-X$ in the low-frequency region.

The results of HgSb are given in Fig. 10. Hg and Sb atoms have almost equal contributions to phonon DOS below 2 THz. From 2 to 4 THz, the vibrations of Hg and Sb atoms are concentrated around 2.2 and 3.1 THz, respectively. The EPC λ remains steadily increasing until 3.5 THz. The results of ZnSb are given in Fig. 11. ZnSb and HgSb display similar electronic DOS. For ZnSb, Zn and Sb contribute to both high- and low-frequency vibrations, such as CuSb. The EPC λ is mainly contributed by the low-frequency vibration modes at point L, high-symmetry paths $K-\Gamma$, and $\Gamma-X$.

V. SUMMARY

To summarize, we have found eight new stable transition metal pnictide superconductors by the first-principle calculations. Among these superconductors, CuN is found to have the strongest EPC of 3.099 and the highest T_c of 30 K. Considering the high-symmery crystal structure, we have obtained

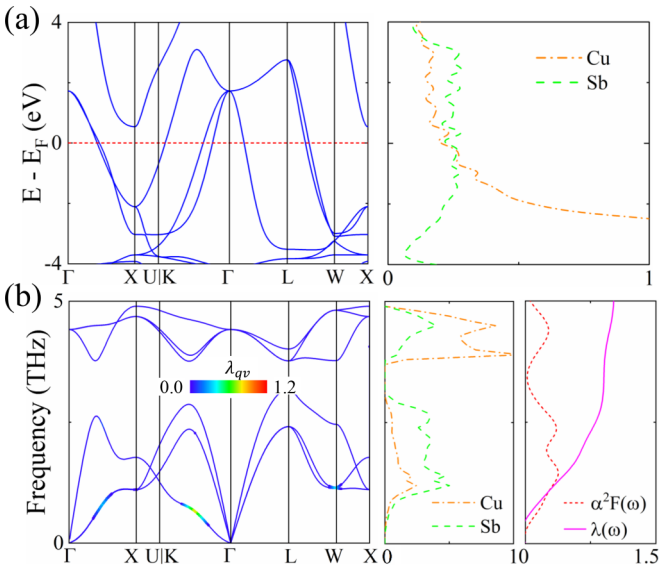

FIG. 9. Same as Fig. 5 but for CuSb.

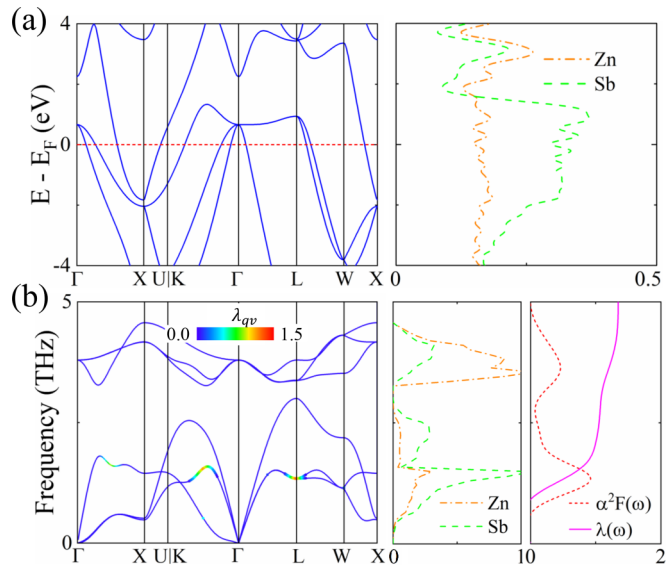

FIG. 11. Same as Fig. 5 but for ZnSb.

the quadratic contact point at Γ where the band dispersion is quadratic along all three directions in k space. Besides, the Weyl loop on the $k_{x/y/z} = 0$ plane and the Weyl points on the $k_{x/y/z} = 2\pi/a$ plane have also been uncovered, indicating the topological properties of CuN. The Weyl point is protected by the C_2 rotation symmetry and time-reversal symmetry and is robust against the effect of SOC. In contrast to ZrN, we find that the softening acoustic phonon models in CuN are responsible for the much higher EPC strength and the much higher T_c. By studying the relationship between T_c and pressure, we find that both ZrN and CuN match well with the BCS superconducting mechanism. Our results not only predict CuN having the highest T_c in TMN superconductors, but also offer new materials with both superconductivity and novel topology in band structures that would be helpful for studying Majorana zero modes in topological quantum computation.

ACKNOWLEDGMENTS

This work was supported, in part, by the National Key R&D Program of China (Grant No. 2018YFA0305800), the Strategic Priority Research Program of the Chinese Academy of Sciences (Grant No. XDB28000000), the National Natural Science Foundation of China (Grant No. 11834014), and Beijing Municipal Science and Technology Commission (Grant No. Z118100004218001). B.G. was supported, in part, by the National Natural Science Foundation of China (Grants No. 12074378 and No. Y81Z01A1A9), the Chinese Academy of Sciences (Grants No. YSBR-030 and No. Y929013EA2), the Strategic Priority Research Program of Chinese Academy of Sciences (Grant No. XDB33000000), and the Beijing Natural Science Foundation (Grant No. Z190011). Innovation Program for Quantum Science and Technology (No. 2021ZD0301800).

[1] S.-H. Jhi, J. Ihm, S. G. Louie, and M. L. Cohen, Nature (London) **399**, 132 (1999).
[2] A. Zerr, G. Miehe, and R. Riedel, Nature Mater. **2**, 185 (2003).
[3] M. Chhowalla and H. E. Unalan, Nature Mater. **4**, 317 (2005).
[4] J. C. Crowhurst, A. F. Goncharov, B. Sadigh, C. L. Evans, P. G. Morrall, J. L. Ferreira, and A. J. Nelson, Science **311**, 1275 (2006).
[5] W. Jin, W. Sun, X. Kuang, C. Lu, and L. Kou, J. Phys. Chem. Lett. **11**, 9643 (2020).
[6] Y. Zou, X. Qi, C. Zhang, S. Ma, W. Zhang, Y. Li, T. Chen, X. Wang, Z. Chen, D. Welch, P. Zhu, B. Liu, Q. Li, T. Cui, and B. Li, Sci. Rep. **6**, 22330 (2016).
[7] L. Chatelain, E. Louyriac, I. Douair, E. Lu, F. Tuna, A. J. Wooles, B. M. Gardner, L. Maron, and S. T. Liddle, Nat. Commun. **11**, 337 (2020).
[8] F. Rivadulla, M. Bañobre-López, C. X. Quintela, A. Piñeiro, V. Pardo, D. Baldomir, M. A. López-Quintela, J. Rivas, C. A. Ramos, H. Salva, J.-S. Zhou, and J. B. Goodenough, Nature Mater. **8**, 947 (2009).
[9] M. Wu, X. Lin, Y. Wang, L. Wang, W. Guo, D. Qi, X. Peng, A. Hagfeldt, M. Grätzel, and T. Ma, J. Am. Chem. Soc. **134**, 3419 (2012).
[10] R. Ningthoujam and N. Gajbhiye, Prog. Mater. Sci. **70**, 50 (2015).
[11] D. A. Papaconstantopoulos, W. E. Pickett, B. M. Klein, and L. L. Boyer, Phys. Rev. B **31**, 752 (1985).
[12] J.-Y. You, B. Gu, G. Su, and Y. P. Feng, Phys. Rev. B **103**, 104503 (2021).
[13] B. T. Matthias and J. K. Hulm, Phys. Rev. **87**, 799 (1952).
[14] E. I. Isaev, R. Ahuja, S. I. Simak, A. I. Lichtenstein, Y. K. Vekilov, B. Johansson, and I. A. Abrikosov, Phys. Rev. B **72**, 064515 (2005).
[15] W. Weber, Phys. Rev. B **8**, 5093 (1973).
[16] X.-J. Chen, V. V. Struzhkin, Z. Wu, M. Somayazulu, J. Qian, S. Kung, A. N. Christensen, Y. Zhao, R. E. Cohen, H. kwang Mao, and R. J. Hemley, Proc. Natl. Acad. Sci. USA **102**, 3198 (2005).
[17] W. Lu, H. Zhai, Q. Li, and C. Chen, J. Phys. Chem. Lett. **12**, 1985 (2021).
[18] B. O. Johansson, J.-E. Sundgren, J. E. Greene, A. Rockett, and S. A. Barnett, J. Vac. Sci., Technol. A **3**, 303 (1985).
[19] B. W. Roberts, J. Phys. Chem. Ref. Data **5**, 581 (1976).
[20] L. Toth, *Transition Metal Carbides and Nitrides* (Elsevier, Amsterdam, 2014).
[21] K. Reichelt, W. Nellen, and G. Mair, J. Appl. Phys. **49**, 5284 (1978).
[22] W. Pickett, B. Klein, and D. Papaconstantopoulos, Physica B+C **107**, 667 (1981).
[23] W. Tsai, M. Delfino, J. A. Fair, and D. Hodul, J. Appl. Phys. **73**, 4462 (1993).
[24] Y. Nishi, S. Tokunaga, and S. Moriya, J. Mater. Sci. Lett. **6**, 1450 (1987).
[25] E. Soignard, P. F. McMillan, T. D. Chaplin, S. M. Farag, C. L. Bull, M. S. Somayazulu, and K. Leinenweber, Phys. Rev. B **68**, 132101 (2003).
[26] D. Papaconstantopoulos, W. Pickett, B. Klein, and L. Boyer, Nature (London) **308**, 494 (1984).
[27] W. Spengler, R. Kaiser, A. N. Christensen, and G. Muller-Vogt, Phys. Rev. B **17**, 1095 (1978).
[28] R. S. Ningthoujam, N. Sudhakar, K. P. Rajeev, and N. S. Gajbhiye, J. Appl. Phys. **91**, 6051 (2002).
[29] N. Sudhakar, R. S. Ningthoujam, K. P. Rajeev, A. K. Nigam, J. Weissmüller, and N. S. Gajbhiye, J. Appl. Phys. **96**, 688 (2004).
[30] N. Gajbhiye and R. Ningthoujam, Mater. Res. Bull. **41**, 1612 (2006).
[31] F. Chen, X. Bai, Y. Wang, T. Dong, J. Shi, Y. Zhang, X. Sun, Z. Wei, M. Qin, J. Yuan *et al.*, arXiv:2201.04340.
[32] G. Kresse and J. Furthmuller, Phys. Rev. B **54**, 11169 (1996).
[33] P. Giannozzi, S. Baroni, N. Bonini, M. Calandra, R. Car, C. Cavazzoni, D. Ceresoli, G. L. Chiarotti, M. Cococcioni, I. Dabo, A. D. Corso, S. de Gironcoli, S. Fabris, G. Fratesi, R. Gebauer, U. Gerstmann, C. Gougoussis, A. Kokalj, M. Lazzeri, L. Martin-Samos *et al.*, J. Phys.: Condens. Matter **21**, 395502 (2009).
[34] P. E. Blochl, Phys. Rev. B **50**, 17953 (1994).
[35] J. P. Perdew, K. Burke, and M. Ernzerhof, Phys. Rev. Lett. **77**, 3865 (1996).

[36] S. Baroni, S. de Gironcoli, A. D. Corso, and P. Giannozzi, Rev. Mod. Phys. **73**, 515 (2001).

[37] D. Vanderbilt, Phys. Rev. B **41**, 7892 (1990).

[38] See Supplemental Material at http://link.aps.org/supplemental/10.1103/PhysRevB.108.014501 for convergence of calculations, SOC effect on superconducting, and topological properties, structure search using CALYPSO, and softening acoustic phonon which includes Refs. [44–47].

[39] M. Methfessel and A. T. Paxton, Phys. Rev. B **40**, 3616 (1989).

[40] G. Güntherodt, J. Phys. Colloques **41**, C5-65 (1980).

[41] F. Giustino, Rev. Mod. Phys. **89**, 015003 (2017).

[42] P. B. Allen and R. C. Dynes, Phys. Rev. B **12**, 905 (1975).

[43] W. L. McMillan, Phys. Rev. **167**, 331 (1968).

[44] Y. Wang, J. Lv, L. Zhu, and Y. Ma, Phys. Rev. B **82**, 094116 (2010).

[45] F. Gulo, A. Simon, J. Köhler, and R. K. Kremer, Angew. Chem. Int. Ed. **43**, 2032 (2004).

[46] I. Agrell, E. von Sydow, T. Kujanpää, B. von Hofsten, D. H. Williams, E. Bunnenberg, C. Djerassi, and R. Records, Acta Chem. Scand. **20**, 1281 (1966).

[47] A. Jain, S. P. Ong, G. Hautier, W. Chen, W. D. Richards, S. Dacek, S. Cholia, D. Gunter, D. Skinner, G. Ceder, and K. A. Persson, APL Mater. **1**, 011002 (2013).

[48] J.-Y. You, B. Gu, and G. Su, Phys. Rev. B **101**, 184521 (2020).

[49] X.-W. Yi, Z. Zhang, Z.-W. Liao, X.-J. Dong, J.-Y. You, and G. Su, Nano Today **42**, 101346 (2022).

[50] J.-Y. You, X.-L. Sheng, and G. Su, Phys. Rev. B **103**, 165143 (2021).

[51] X.-L. Qi and S.-C. Zhang, Rev. Mod. Phys. **83**, 1057 (2011).

[52] W.-H. Dong, Y.-Y. Zhang, Y.-F. Zhang, J.-T. Sun, F. Liu, and S. Du, npj Comput. Mater. **8**, 185 (2022).

[53] J.-F. Zhang, P.-J. Guo, M. Gao, K. Liu, and Z.-Y. Lu, Phys. Rev. B **99**, 045110 (2019).

[54] J.-Y. You, B. Gu, G. Su, and Y. P. Feng, J. Am. Chem. Soc. **144**, 5527 (2022).

[55] Z. Zhang, J.-Y. You, B. Gu, and G. Su, Phys. Rev. B **106**, 174519 (2022).

[56] X.-W. Yi, X.-Y. Ma, Z. Zhang, Z.-W. Liao, J.-Y. You, and G. Su, Phys. Rev. B **106**, L220505 (2022).

[57] X.-J. Chen, V. V. Struzhkin, S. Kung, H. K. Mao, R. J. Hemley, and A. N. Christensen, Phys. Rev. B **70**, 014501 (2004).

[58] J. S. Schilling, in *Handbook of High-Temperature Superconductivity* (Springer, Berlin, 2007), pp. 427–4620.

[59] J. Hopfield, Physica **55**, 41 (1971).

[60] X. J. Chen, H. Zhang, and H.-U. Habermeier, Phys. Rev. B **65**, 144514 (2002).

[61] G. Xu, B. Lian, P. Tang, X.-L. Qi, and S.-C. Zhang, Phys. Rev. Lett. **117**, 047001 (2016).

[62] S. Zhu, L. Kong, L. Cao, H. Chen, M. Papaj, S. Du, Y. Xing, W. Liu, D. Wang, C. Shen, F. Yang, J. Schneeloch, R. Zhong, G. Gu, L. Fu, Y.-Y. Zhang, H. Ding, and H.-J. Gao, Science **367**, 189 (2020).

[63] D. Wang, L. Kong, P. Fan, H. Chen, S. Zhu, W. Liu, L. Cao, Y. Sun, S. Du, J. Schneeloch, R. Zhong, G. Gu, L. Fu, H. Ding, and H.-J. Gao, Science **362**, 333 (2018).

[64] P. Zhang, K. Yaji, T. Hashimoto, Y. Ota, T. Kondo, K. Okazaki, Z. Wang, J. Wen, G. D. Gu, H. Ding, and S. Shin, Science **360**, 182 (2018).

[65] C.-K. Chiu, T. Machida, Y. Huang, T. Hanaguri, and F.-C. Zhang, Sci. Adv. **6**, eaay0443 (2020).

[66] W. Liu, L. Cao, S. Zhu, L. Kong, G. Wang, M. Papaj, P. Zhang, Y.-B. Liu, H. Chen, G. Li, F. Yang, T. Kondo, S. Du, G.-H. Cao, S. Shin, L. Fu, Z. Yin, H.-J. Gao, and H. Ding, Nat. Commun. **11**, 5688 (2020).

[67] L. Kong, L. Cao, S. Zhu, M. Papaj, G. Dai, G. Li, P. Fan, W. Liu, F. Yang, X. Wang, S. Du, C. Jin, L. Fu, H.-J. Gao, and H. Ding, Nat. Commun. **12**, 4146 (2021).

[68] M. Li, G. Li, L. Cao, X. Zhou, X. Wang, C. Jin, C.-K. Chiu, S. J. Pennycook, Z. Wang, and H.-J. Gao, Nature (London) **606**, 890 (2022).

[69] Z. Liang, X. Hou, F. Zhang, W. Ma, P. Wu, Z. Zhang, F. Yu, J.-J. Ying, K. Jiang, L. Shan, Z. Wang, and X.-H. Chen, Phys. Rev. X **11**, 031026 (2021).